Asian Journal of Chemistry; Vol. 34, No. 5 (2022), 1237-1244

ASIAN JOURNAL OF CHEMISTRY

https://doi.org/10.14233/ajchem.2022.23697


# Purification of Crude Bentonite Clay: Synthesis and Characterization of Na, Mg and Cu Incorporated Bentonite Clay

DEBASIS BORAH, HARSHAJIT NATH and HEMAPROBHA SAIKIA*

Department of Chemistry, Bodoland University, Rangalikhata, Deborgaon-783370, India

*Corresponding author: E-mail: saikiahemaprobha@gmail.com

*Received*: 1 January 2022; *Accepted*: 27 February 2022; *Published online*: 20 April 2022; AJC-20777

Commercially available natural bentonite clay samples obtained from Oil India Limited, India, were purified *via* standard sedimentation process followed by screening with the help of siphoning process by applying Stock's law to obtain < 2 µm fraction of the clay. The $Na^+$, $Mg^{2+}$ and $Cu^{2+}$ cations were incorporated in the interlayers of the bentonite clay by applying different chemical procedures. Modified bentonite clays thus obtained were characterized by PXRD, HRTEM, FTIR analysis, DRS analysis, TGA, SEM & EDX analysis, and BET surface area analysis.

**Keywords: Bentonite, Purification, Incorporation, Modification.**

## INTRODUCTION

Bentonite is a smectic group clay that is mainly aluminum phyllosilicate and primarily composed of montmorillonite, having hydrated sodium, calcium, magnesium and aluminum silicate. In addition to these, it contains a small portion of quartz, feldspar, volcanic glass, organic matter, gypsum or pyrite [1]. Bentonite is a layer structured clay whose basic structure is composed of tetrahedral lattice structure containing $Si^{4+}$ ion at the center surrounded by $O^{2-}$ ions at the corners of the tetrahedron and octahedral lattice unit containing $Al^{3+}$ ion at the center of the lattice surrounded by $OH^-$ ions at the corners of the octahedral [2], which has a 2:1 type silica structure [3].

The typical swelling property exhibited by bentonite clay makes its greatest use in the industry [4]. Water and other polar molecules can enter between the unit layers of bentonite clay in the direction, which is normal to the basal plane resulting from the expansion of the structure of the clay [5]. The overall net negative charge of silica-alumina units of bentonite cause a great affinity for metallic cations [6]. Depending on the water to clay ratio, bentonite clay can exhibit adhesion property, plastic property, and lubricating property [7]. Thus bentonite clay is used widely in the field of drilling for the preparation of drilling fluid, foundry sand binding, iron ore pelletizing, water proofing and sealant, *etc*. [8,9].

Due to the presence of a net negative charge, natural bentonite clay is although good sorbent of water and cationic molecules but the net negative charge limits its sorption capacity to anionic and non-ionic molecules. To increase the functionality of bentonite clay, the surface charge can be changed by incorporating more cations in the interlayer spacing of the clay or by modifying with organic surfactants [10]. By these methods, greater interlayer spacing of bentonite clay can be achieved by hydrogen bonding between oxides and silicate surface [11]. Metal cation incorporated bentonite clay can be used as a heterogeneous catalyst and has advantages over the natural bentonite clay as they are less toxic [12], highly selective, non-corrosive, and easy to work up [13].

In this study, we aimed to synthesize $Na^+$, $Mg^{2+}$ and $Cu^{2+}$ modified bentonite clay and characterized leads to understand the changes in the structural and textural properties, which are crucial to determine their applications.

## EXPERIMENTAL

Commercially available bentonite clay was collected from Oil India Limited, Duliajan, India. All the commercial reagents and solvents were used without further purification and supplied by Zenith India Ltd. and Merck, India.

**Purification of crude bentonite clay:** Commercially available bentonite clay powder was dispersed in distilled water

using a magnetic stirrer in a 1L beaker for 1 h to make 2% suspension of the clay. Using standard sedimentation siphoning process and following Stock's law, < 2 µm fraction of the clay was separated. The impurities which are generally present in crude bentonite clay such as quartz, calcite, beotite, feldspar, cristobalite, kaolinite, mica, organic matter, *etc*. were settled down and the top suspension of the clay was siphoned off in another beaker. The suspension was poured into Petri dishes and allowed to dry in an air oven at 60 ºC. The dried clay from Petri dishes was transferred in well-stoppered bottles and stored in a desiccator.

**Synthesis of Na-modified bentonite clay:** Purified bentonite clay (2 g) was dispersed in 100 mL of distilled water and stirred for 1 h by using a magnetic stirrer. A NaCl solution (100 mL of 2M) was added to this solution and stirred overnight. The suspension was then allowed to settle down for one day. The clear suspension was decanted and the remaining suspension was again stirred with 100 mL of 2 M NaCl solution. This process of stirring, settling and decantation was repeated to ensure complete exchange of cations such as $Ca^{2+}$, $Mg^{2+}$, *etc*. with $Na^+$ ions. The suspension was then centrifuged and washed several times with distilled water to remove excess $Na^+$ ions. The complete removal of excess $Na^+$ ions was checked by the $AgNO_3$ test for $Cl^-$ ions. Finally, when clay stopped settling down, the suspension was transferred in a dialysis bag and dipped in distilled water contained in a 1000 mL beaker. Water in the beaker was replaced 6 hourly till it showed no test for $Cl^-$ ions by $AgNO_3$ test. The suspension was then transferred to a petri dish and dried in an air oven at 600 ºC. The flakes of Na-bentonite obtained were transferred in well stoppered bottled and stored in a desiccator.

**Synthesis of Mg-modified bentonite clay:** Purified bentonite clay (10 g) was mixed with 100 mL of 1.25 M $MgCl_2$ solution and the mixture was stirred for 6 h. After stirring, the above solution was transferred into a glass Petri dish and dried at 150 ºC in an air oven. The dried mass was then grounded to a fine powder and was calcined at 450 ºC for 4 h in a muffle furnace. The calcined powder was cooled to room temperature and washed twice with distilled water in a 1:20 ratio. The material was finally dried at 70 ºC for 6 h and the yield was recorded.

**Synthesis of Cu-modified bentonite clay:** A quantity of purified bentonite clay was added to ultrapure water at room temperature and then stirred for about 0.5 h at 300 rpm/min. A copper hydroxide solution was prepared by adding NaOH pellets to copper chloride with an OH/Cu ratio of 2:1. Now added this solution slowly to the bentonite clay solution and then stirred at room temperature for 15 h, centrifuged at 3000 tr/min for 10 min and finally washed several times with distilled water to remove the excess chlorides. The recovered product was oven-dried at 110 ºC for 24 h. The solid was finally calcined at 425 ºC and stored in a desiccator.

## RESULTS AND DISCUSSION

**PXRD analysis:** The PXRD curves for purified bentonite (Pure B), sodium incorporated bentonite (Na-B), copper incorporated (Cu-B) and magnesium incorporated bentonite (Mg-B) is shown in Fig. 1. The PXRD pattern of purified bentonite clay indicates the presence of impurities such as quartz, hematite and calcite. Quartz reflections corresponding to 2θ: 20.850º, 26.652º, 36.542º, hematite reflections to 2θ: 24.138º, 33.153º, 35.612º and calcite reflections 2θ: 23.022º, 29.406º. This clay mineral can be identified by the peaks appearing on 2θ at 20.801º and 35.405º, which matched the structure of beidellite. Beideillite and bentonite both belong to the smectic (2:1 sheet type) clays.

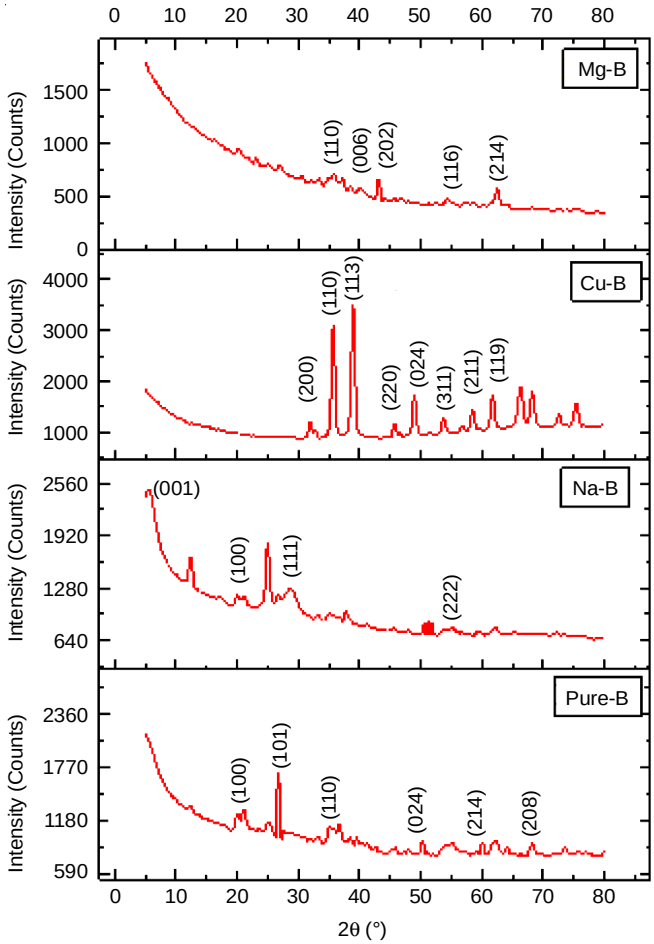


Fig. 1. PXRD curves for purified bentonite (Pure-B), sodium incorporated bentonite (Na-B), copper incorporated (Cu-B) and magnesium incorporated bentonite (Mg-B)

The Na incorporated bentonite XRD pattern represents the $d_{001}$ with basel spacing 15.58Å, located at 5.67º, which indicates that the montmorillonite clay mineral is predominant in bentonite clay [14]. The patterns showed the presence of different peaks corresponding to planes (100) and (202) indicating the presence of quartz, the peak corresponding to the plane (111) indicates the presence of silicon as impurities.

The XRD pattern of Mg modified bentonite does not contains the $d_{001}$ plan. The absence of (001) peak in the lower region is due to the lack of sufficiently ordered silicate layer structure. The data showed the presence of impurities such as hematite (35.84º, 38.1º, 43.18º, 54.74º and 62.47º) and calcite (58.8º and 65.9º). Finally, the XRD pattern of Cu-modified bentonite also does not contain the $d_{001}$ plan. The absence of (001) peak in the lower region is due to the lack of sufficiently

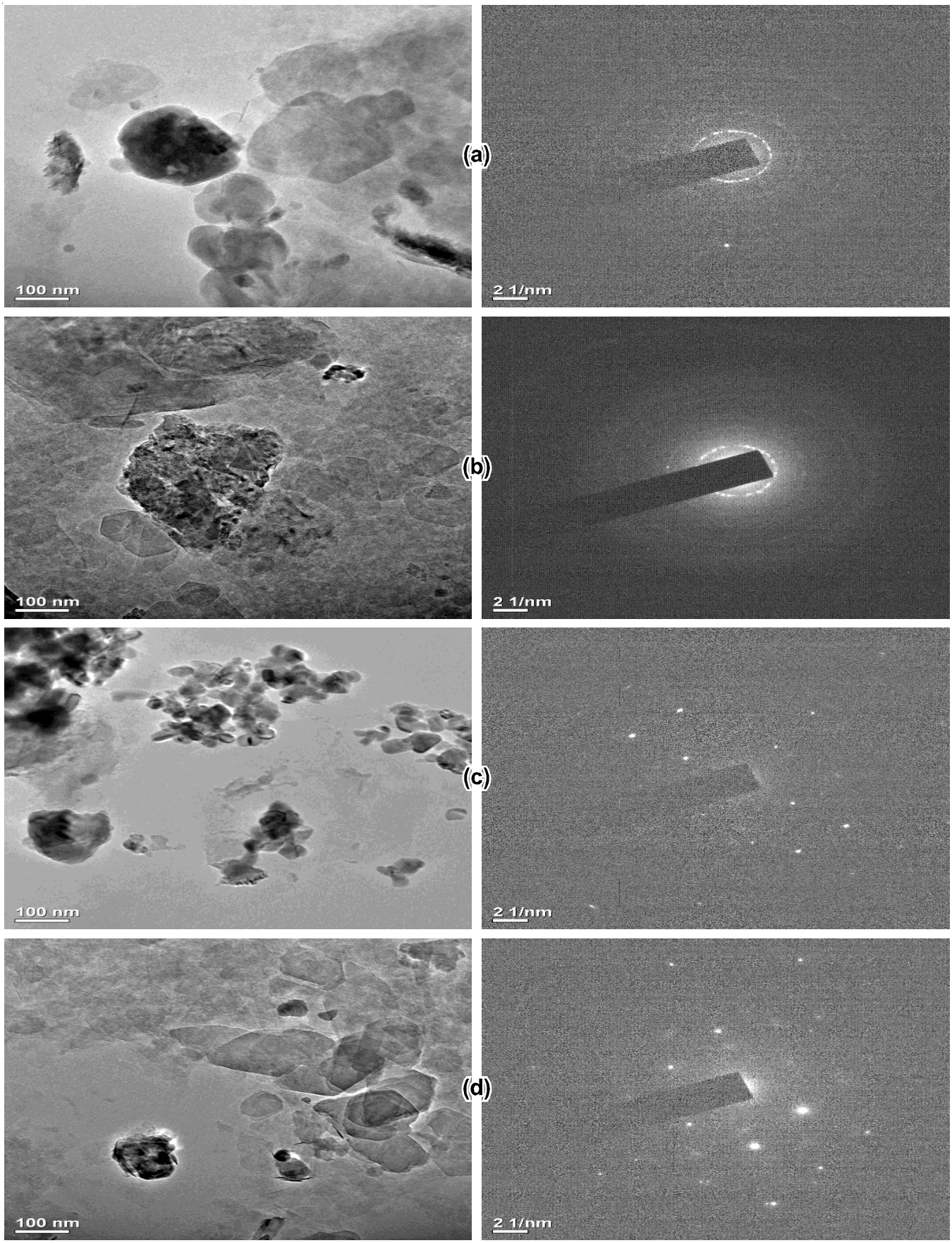


Fig. 2. HRTEM images along with SAED pattern of (a) Purified bentonite clay, (b) Na-bentonite clay, (c) mg-bentonite clay and (d) Cu-bentonite clay

ordered silicate layer structure. The data showed the presence of impurities such as halite (31.957º, 45.64º, 53.67º and 56.71º), hematite (32.73º, 35.729º and 48.915º), calcite (38.913º and 61.721º) and quartz (58.42º).

**HRTEM analysis:** Bright-field TEM images for purified bentonite, Na-bentonite, Mg-bentonite and Cu-bentonite are shown in Fig. 2 along with their SAED Patterns. It is noticed that purified bentonite clay and other metal incorporated clays contain several clusters of different sizes and shapes, where layers are dispersed randomly in either elongated or coiled form. The dark spheres represent both $Fe_2O$ and $Al_2O_3$. The ionic size of $Fe^{3+}$ (0.64 Å) is larger than that of $Al^{3+}$ (0.50 Å), so the larger spheres are due to the presence of $Fe_2O$ and smaller spheres are observed due to the presence of $Al_2O_3$.

The planes and inter-planar spacing were characterized using the SAED pattern of the prepared samples. The SAED pattern of all the prepared samples exhibits circular and semi-circular rings corresponding to common (100), (110) crystallographic planes with *d*-values 4.25 and 2.49, respectively. The incorporated Na-B, Cu-B, and Mg-B also contain some other crystallographic planes like (220) and (410). This result demonstrates that the prepared materials are crystalline and it also confirmed that the incorporated bentonite clays were successfully synthesized.

**FTIR analysis:** The FTIR curves for purified bentonite (Pure-B), sodium incorporated bentonite (Na-B), copper incorporated (Cu-B) and magnesium incorporated bentonite (Mg-B) is shown in Fig. 3. The FTIR spectrum of purified bentonite recorded in the range 4000 to 500 $cm^{-1}$ and the main absorption bands with their corresponding assignments are shown in Table-1.

A sharp band observed at 3787 $cm^{-1}$ is assigned to Al-O-Al in the clay. A single band observed at 3644 $cm^{-1}$ followed by broad band at 3384 $cm^{-1}$ in the clay is assigned to OH stretching ($\nu_3$) of structural hydroxyl group and water present in the clay [1]. This indicates the possibility of hydroxyl linkage between octahedral and tetrahedral layers. The band observed at 3164 $cm^{-1}$ may be attributed to the presence of the C-H group. A sharp and intense band observed at 1640 $cm^{-1}$ is due to the asymmetric OH stretch (deformation mode) of water, which

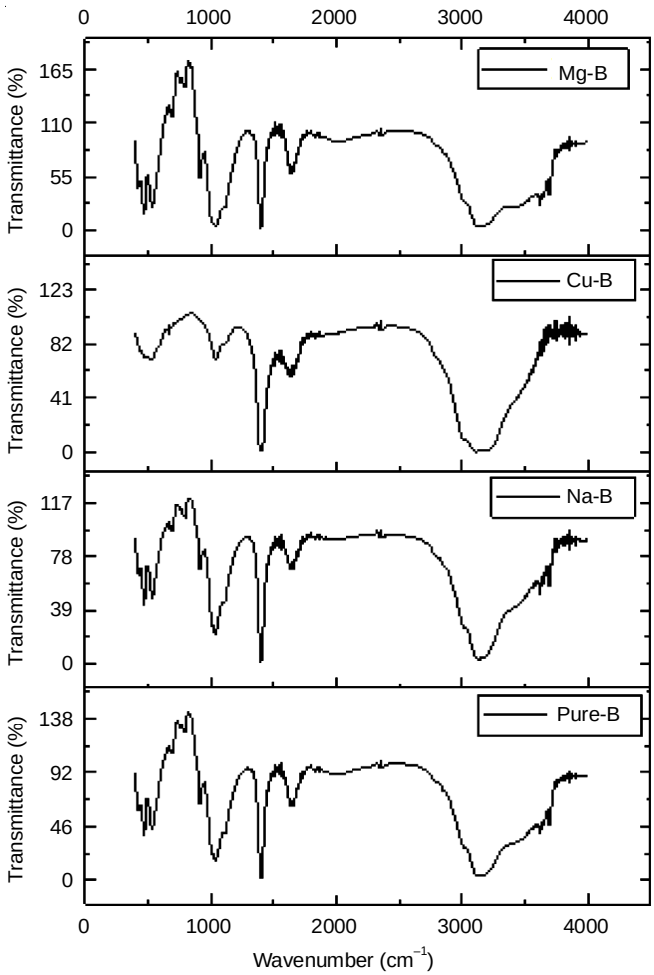


Fig. 3. FTIR curves for purified bentonite (Pure-B), sodium incorporated bentonite (Na-B), copper incorporated (Cu-B) and magnesium incorporated bentonite (Mg-B)

is the structural part of clay. A very sharp and intense absorption band at 1401 $cm^{-1}$ is characteristic of carbonates. The band around 1026 $cm^{-1}$ corresponds to the asymmetric stretching vibrations of $SiO_2$ tetrahedra [2]. The band observed at 768 $cm^{-1}$ corresponds to O-H stretching mode. The band observed at 536 $cm^{-1}$ corresponds to the deformation mode of the Al-O-Si group.

TABLE-1
FTIR WAVENUMBERS WITH THEIR ATTRIBUTIONS FOR PURIFIED BENTONITE CLAY, Na-BENTONITE CLAY, Mg-BENTONITE CLAY AND Cu-BENTONITE CLAY

| Purified bentonite clay | | Na-bentonite clay | | Mg-bentonite clay | | Cu-bentonite clay | |
|---|---|---|---|---|---|---|---|
| Wavenumber ($cm^{-1}$) | Attribution | Wavenumber ($cm^{-1}$) | Attribution | Wavenumber ($cm^{-1}$) | Attribution | Wavenumber ($cm^{-1}$) | Attribution |
| 3787 | Al-OH-Al | 3760 | Al-OH-Al | 3763 | Al-OH-Al | 3691 | Al-O-Al |
| 3644 | Asym. O-H *str.* ($\nu_3$) | 3571 | O-H *str.* | 3614 | O-H *str.* | 3432 | H-O-H |
| 3384 | H-O-H | 3150 | C-H group | 3408 | H-O-H | 3159 | C-H group |
| 3164 | C-H group | 1642 | O-H *str.* | 3140 | C-H group | 1630 | O-H *str.* |
| 1640 | O-H *str.*. | 1394 | Carbonates | 1635 | Asym. OH *str.* | 1408 | Carbonates |
| 1401 | Carbonates | 1008 | Si-O *str.* | 1391 | Carbonates | 1036 | Si-O *str.* |
| 1026 | Si-O *str.* | 758 | O-H *str.* | 1021 | Si-O *str.* | 552 | Al-O-Si |
| 768 | O-H *str.* | 643 | Al-Fe-Mg OH deformation | 897 | Al-Fe-Mg OH deformation | | |
| 536 | Al-O-Si | 523 | Si-O-Al | 768 | Si-O | | |
| | | | | 686 | Size | | |
| | | | | 519 | Al-O-Si | | |

The FTIR spectrum of Na-incorporated bentonite clay exhibited four bands at 3760, 3571, 1642 and 758 $cm^{-1}$ were assigned to stretching vibrations of water-adsorbed molecules and the exchangeable cations. Furthermore, the water molecules exhibited fundamental vibration modes, *viz.* symmetric stretching and H-O-H bending. The band observed at 3150 $cm^{-1}$ may be attributed to the C-H group. The typical bands for the silicate components of the clay appear between 1200 and 400 $cm^{-1}$. The band at 1008 $cm^{-1}$ is due to the in-plane band stretching of Si-O bonds. the band at 523 $cm^{-1}$ can be attributed to Si-O-Al species.

The FTIR spectrum of Mg-incorporated bentonite clay also exhibited the four bands at 3763, 3614, 3408 and 1635 $cm^{-1}$ were assigned to stretching vibrations of water-adsorbed molecules and the exchangeable cations. Furthermore, the water molecules exhibited fundamental vibration modes, *viz.* symmetric stretching and H-O-H bending. The band observed at 3140 $cm^{-1}$ may be attributed to the C-H group. The absorption band observed at 1391 $cm^{-1}$ attributed due to the presence of carbonates. The typical bands for the silicate components of the clay appear between 1200 and 400 $cm^{-1}$. The band at 1008 $cm^{-1}$ is due to the in-plane band stretching of Si-O bonds. The bands observed at 897 and 768 $cm^{-1}$ are due to the vibrational modes of $SiO_2$ tetrahedron. The band at 519 $cm^{-1}$ can be attributed to Si-O-Al species.

The FTIR spectrum of Cu-incorporate bentonite exhibited two the absorption bands at 3691 and 3432 $cm^{-1}$, which is be attributed to the asymmetric and symmetric stretching of structural hydroxyl groups. The band observed at 3159 $cm^{-1}$ may be attributed to the presence of the C-H group. An absorption band at 1630 $cm^{-1}$ attributed to the angular vibration of the -OH group and related to the adsorbed water and hydration water present in the clay. A distinctive band is also observed in the copper-modified bentonite at 1408 $cm^{-1}$, which can be attributed to the presence of carbonates. A characteristic Si-O bond can be observed at 1036 $cm^{-1}$. The absorption band at 552 $cm^{-1}$ is attributed to the Si-O-Si bending vibration.

**UV-Vis DRS analysis:** The UV-Vis DRS study of pure-B, Na-B, Cu-B and Mg-B is shown in Fig. 4. The absorption spectra are difficult to interpret as the powder sample diffuses a large amount of light with a large thickness. To avoid this difficulty, diffusion reflectance spectroscopy and Schuster-Kubelka-Munk (SKM) relation is used to correlate diffused reflectance to the absorption coefficient.

To determine the direct bandgap energy, a plot of photon energy, eV is drawn against in atomic units (Fig. 5). The direct bandgap for pure-B, Na-B, Cu-B and Mg-B were found to be 0.76, 0.75, 0.82 and 0.56 eV, respectively. In the case of the determination of indirect bandgap energy, a plot of photon energy, eV is drawn against and the indirect band gaps for pure-B, Na-B, Cu-B, and Mg-B were found to be 0.73, 0.69, 0.78 and 0.30 eV, respectively. The bandgap of the materials has an important role in determining the catalytic and adsorption characteristic properties of the materials. The bandgap energies of the prepared samples are found to be different from each other due to particle size and shape.

**TGA analysis:** The TGA curves for raw or pure bentonite (Pure-B), sodium incorporated bentonite (Na-B), copper incorporated (Cu-B) and magnesium incorporated bentonite (Mg-B) is shown in Fig. 6. For pure-B, a curve show a mass loss of approximately 1.68 % occured between 34 and 135 ºC, whereas, the mass loss for Na-B is 1.72 % between 34 and 120 ºC, for Cu-B is 2.57 % between 736 and 925 ºC and for Mg-B is 3.19% at 35 to 281 ºC. In all the cases, this mass loss is probably due to the release of water, which was adsorbed on the surface as well as coordinated to exchangeable cations.

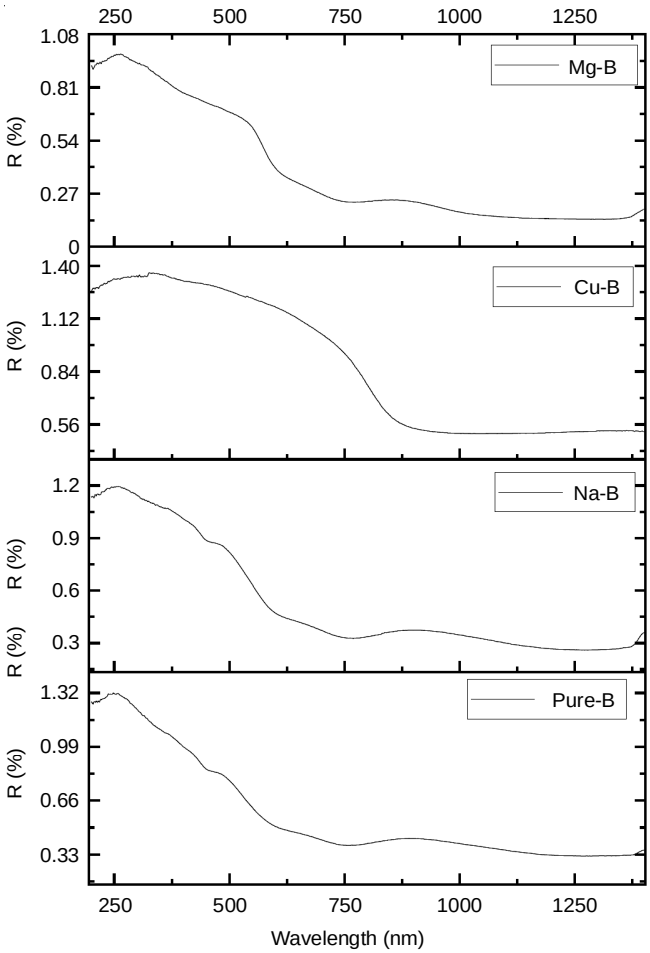


Fig. 4. UV-Vis DRS spectra of Pure-B, Na-B, Cu-B and Mg-B

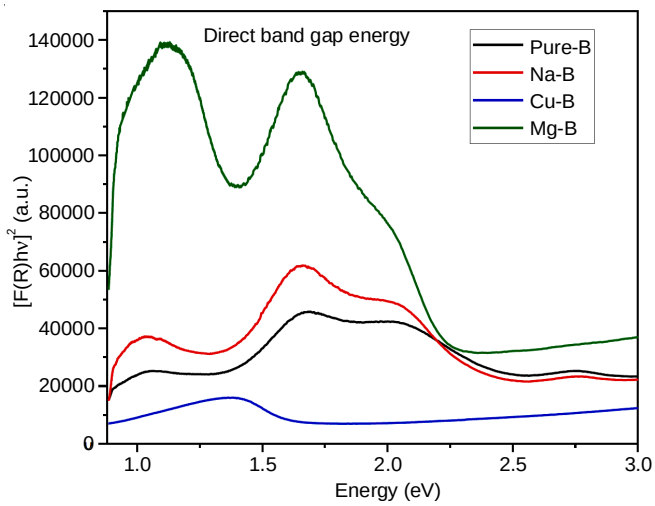


Fig. 5. Direct (left panel) bandgap energy of Pure-B, Na-B, Cu-,B and Mg-B

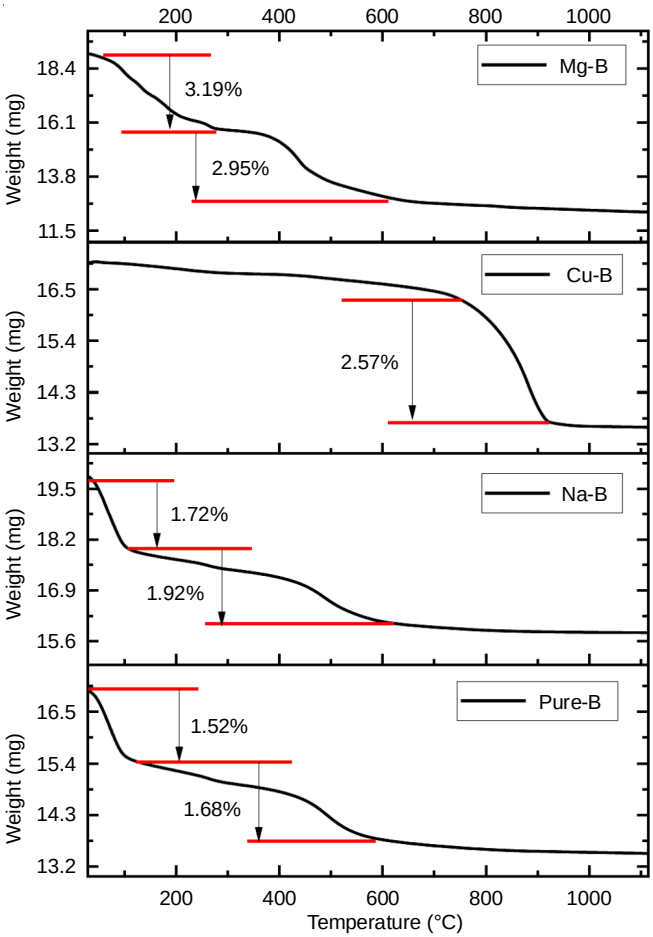


Fig. 6. TGA curves or Pure-B, Na-B, Cu-B and Mg-B

The second mass loss of pure-B was observed at 135 to 567 ºC is due to decarboxylation of montmorillonite clay with high iron content. The second mass loss for modified Na-B and Mg-B (Table-2) is due to the decarboxylation and decomposition reactions.

TABLE-2
PERCENTAGE OF MASS LOSS OF PURE-B, Na-B, Cu-B AND Mg-B DURING TGA

| Sample | 1st Mass loss (%) | 2nd mass loss (%) |
|---|---|---|
| Pure-B | 1.52 | 1.68 |
| Na-B | 1.72 | 1.92 |
| Cu-B | 2.57 | – |
| Mg-B | 3.19 | 2.95 |

**SEM and EDX analysis:** The analysis results of the prepared samples by SEM and EDS showed the changes in the morphology of bentonite upon the incorporation of different metal atoms into its interlayer. Fig. 7a represents the purified natural bentonite clay where characteristics smectite texture resembling a tissue layer is visible, but separation zones are not distinct. The morphology of the samples after incorporation with metal ions did not change significantly. This is due to the reason that modifications are mostly intercalated into the interlayer spaces of smectite. Thus typical morphology of montmorillonite is evident. The percentage weight of constituting elements were calculated with the help of EDS, which are given in Table-3.

TABLE-3
ELEMENTAL COMPOSITION OF VARIOUS INCORPORATED BENTONITE CLAY

| Element | Purified bentonite (weight %) | Na-bentonite (weight %) | Mg-bentonite (weight %) | Cu-bentonite (weight %) |
|---|---|---|---|---|
| CK | 0.15 | 0.78 | 0.18 | 0.43 |
| OK | 39.42 | 41.45 | 40.14 | 20.01 |
| NaK | 1.23 | 0.19 | 1.07 | – |
| MgK | 1.59 | 1.25 | 1.34 | 0.43 |
| AlK | 15.25 | 15.28 | 15.29 | 4.87 |
| SiK | 26.58 | 25.90 | 26.59 | 8.45 |
| AuM | 4.24 | 4.58 | 4.00 | 3.81 |
| ClK | 0.46 | 0.41 | 0.93 | 0.64 |
| KK | 0.51 | 0.51 | 0.40 | – |
| CaK | 0.69 | 0.24 | 0.66 | – |
| TiK | 1.60 | 1.42 | 1.54 | – |
| FeK | 8.29 | 7.99 | 7.86 | 3.04 |
| CuK | – | – | – | 58.32 |

**BET surface area analysis:** The BET isotherms of the prepared samples are shown in Fig. 8, these are type IV isotherms and generally shown by mesoporous materials. When capillary condensation occurs, the type IV isotherm will result. Gases condense in the tiny capillary pores of the solid at a pressure below the saturation pressure of the gas. At the lower pressure region, it shows the formation of a monolayer followed by a formation of multilayers. From this analysis, it can be concluded that the surface areas of 48.090, 18.854 and 12.951 $m^2/g$ for Na-B, Cu-B and Mg-B, respectively and their mesoporous nature indicates that the prepared modified bentonite is a good adsorbent (Table-4). The decrease in surface area and pore size are due to the reason that during heating treatment of 200 to 400 ºC (like calcination process) completely collapsed the interlayer, incorporating interlayer cations into the tetrahedral or unoccupied octahedral sites. Calcining temperature for maximizing morbidity, generally, does not exceed the dehydration interval. It is concluded that the decomposition of the 2:1 layers of the clay and collapsing of micro and mesopores by intra- and inter-particle caused a rapid decrease in surface area, volume as the temperature increases.

TABLE-4
SURFACE AREA DISTRIBUTION OF THE PREPARED SAMPLES

| Sample | Surface area ($m^2/g$) | Pore volume ($cm^3\ g^{-1}$) | Pore size (Å) |
|---|---|---|---|
| Pure-B | 21.299 | 0.057 | 40.46 |
| Na-B | 48.090 | 0.063 | 41.86 |
| Cu-B | 18.854 | 0.057 | 40.37 |
| Mg-B | 12.951 | 0.022 | 34.12 |

## Conclusion

It is found that modification to the bentonite clay improves its functionality. The syntheses of functionalized clays such as pillared bentonite clays and porous clay heterostructures introduce the new class of heterostructure materials with improved functionality. Purification of commercially available bentonite clay is carried out and Na, Mg and Cu metal ions were incorporated in the interlayers of this purified bentonite

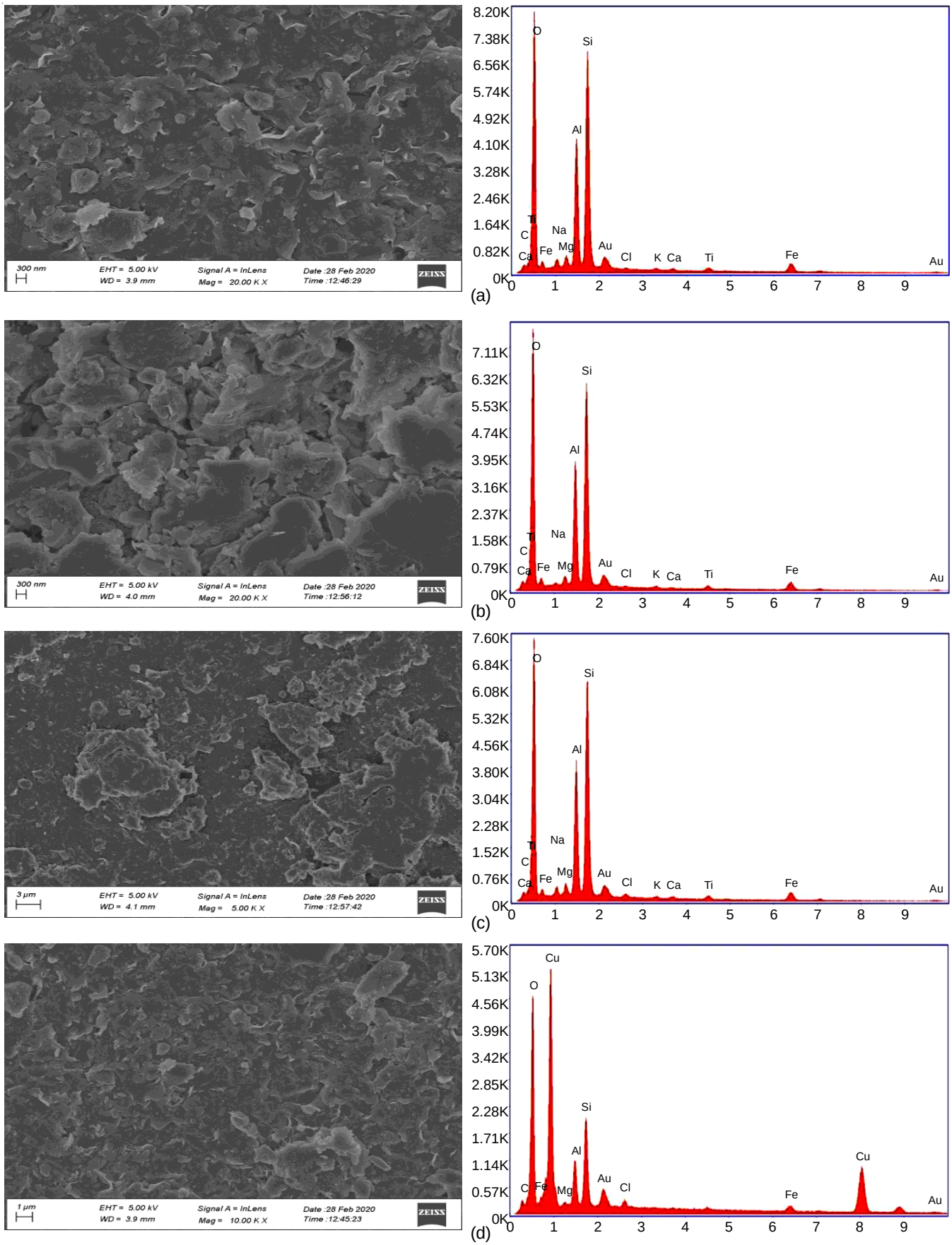


Fig. 7. Scanning electron microscopy (SEM) images of samples: (a) purified bentonite (b) Na-bentonite (c) Mg-bentonite and (d) Cu-bentonite (WD-working distance, Mag-magnification, EHT- electron high tension)

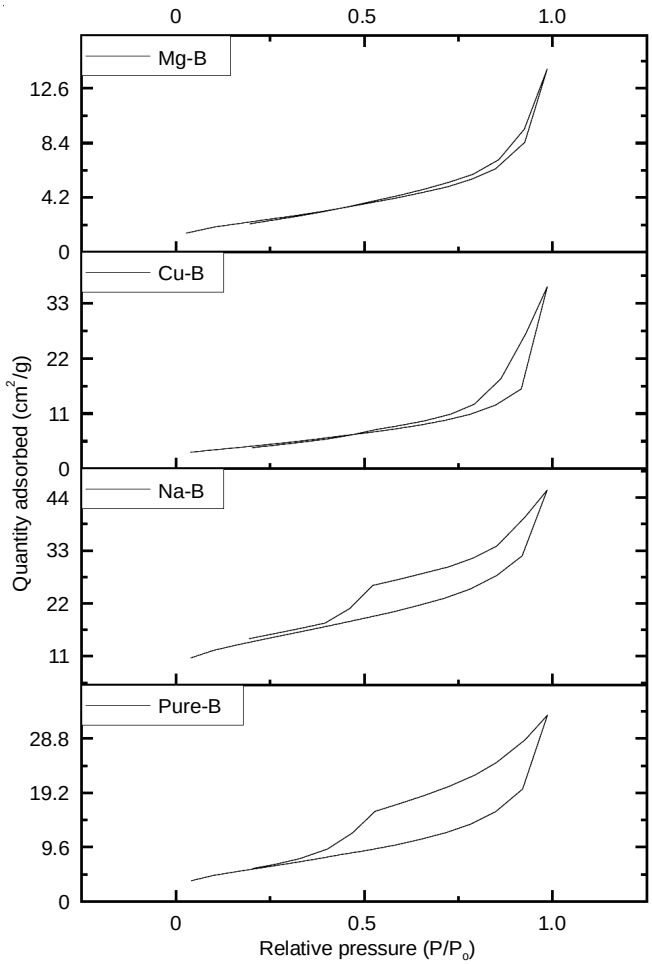


Fig. 8. Nitrogen adsorption isotherm of Pure-B, Na-B, Cu-B and Mg-B

clay. Synthesis of different metal incorporated bentonite clay was confirmed by PXRD, HRTEM, FTIR, DRS, TGA, SEM & EDS and BET surface area analyses.

## CONFLICT OF INTEREST

The authors declare that there is no conflict of interests regarding the publication of this article.

## REFERENCES

1. S. Pandey, *J. Mol. Liq.*, **241**, 1091 (2017); https://doi.org/10.1016/j.molliq.2017.06.115
2. T.R. Reddy, S. Kaneko, T. Endo and S.L. Reddy, *J. Lasers Opt. Photon.*, **4**, 171 (2017); https://doi.org/10.4172/2469-410X.1000171
3. M. Andrunik and T. Bajda, *Materials*, **12**, 3772 (2019); https://doi.org/10.3390/ma12223772
4. A.K. Chaturvedi, K.P. Yadava, K.C. Pathak and V.N. Singh, *Water, Air Soil Pollut.*, **49**, 41 (1990); https://doi.org/10.1007/BF00279509
5. Z.H. Li and R.S. Bowman, *Environ. Eng. Sci.*, **15**, 237 (1998); https://doi.org/10.1089/ees.1998.15.237
6. S. Tian, P. Jiang, P. Ning and Y. Su, *Chem. Eng. J.*, **151**, 141 (2009); https://doi.org/10.1016/j.cej.2009.02.006
7. E.A. Hauser and M.B. Leggett, *J. Am. Chem. Soc.*, **62**, 1811 (1940); https://doi.org/10.1021/ja01864a046
8. J. Konta, *Appl. Clay Sci.*, **10**, 275 (1995); https://doi.org/10.1016/0169-1317(95)00029-4
9. H.A. Patel, R.S. Somani, H.C. Bajaj and R.V. Jasra, *Curr. Sci.*, **92**, 1004 (2007).
10. Y. Zhang, Y. Zhao, Y. Zhu, H. Wu, H. Wang and W. Lu, *J. Environ. Sci.*, **24**, 1525 (2012); https://doi.org/10.1016/s1001-0742(11)60950-9
11. S.M. Lee and D. Tiwari, *Appl. Clay Sci.*, **59-60**, 84 (2012); https://doi.org/10.1016/j.clay.2012.02.006
12. R.B. Achma, A. Ghorbel, A. Dafinov and F. Medina, *Appl. Catal. A*, **349**, 20 (2008); https://doi.org/10.1016/j.apcata.2008.07.021
13. T. Choudhury and N.M. Misra, *Bull. Mater. Sci.*, **34**, 1273 (2011).
14. I. F. Leite, C.M.O. Raposo and S.M.L. Silva, *Cerâmica*, **54**, 331 (2008); https://doi.org/10.1590/S0366-69132008000300006